Ethanol-CVD Growth of Large Single-Crystal Graphene on Flat Cu Surfaces

Andrea Gnisci,[†] Giuliana Faggio,[†] Giacomo Messina,[†] Junyoung Kwon[‡], Jong-Young Lee[‡], Gwan-Hyoung Lee[‡], Theodoros Dikonimos[⁘], Nicola Lisi[⁘], Andrea Capasso[‡,]*

† DIIES Dept.,University "Mediterranea", Via Graziella, Loc. Feo di Vito (Reggio Calabria Italy)

⁘ ENEA, DTE PCU IPSE, Casaccia Research Centre, Via Anguillarese 301 (Rome, Italy)

‡ Department of Materials Science and Engineering, Yonsei University, Seoul 03722, Republic of Korea

ABSTRACT: High-quality graphene can be produced in large scale by chemical vapor deposition (CVD). Ethanol is emerging as a versatile carbon source alternative to methane for the growth of graphene on a copper (Cu) foil catalyst. To date, rigorous studies of the ethanol-based process still lack, especially concerning the first stages of the growth, which ultimately determine graphene's properties, such as defect density and crystal size, and performance, such as electrical conductance

* **Corresponding Author:** *capasso@yonsei.ac.kr (Andrea Capasso).

and mechanical strength. In particular, so far the growth of isolated graphene grains by ethanol-CVD has been obtained only on pre-oxidized Cu foils folded in enclosures, in an attempt to limit the partial pressure of the precursor and thus the nucleation rate. We here systematically explored the process parameters of ethanol-CVD to obtain full control over the nucleation rate, grain size and crystallinity of graphene on flat Cu foils, which are of interest for any realistic production in large scale. In order to limit the nucleation density and increase the grain size, pre-oxidized Cu foils (250 °C in air) were used as substrates, and the process parameters were thoroughly investigated and tuned. Ultimately, at an ethanol vapor flow of 1.5×10^{-3} sccm, the nucleation density was reduced to less than 3 nuclei/mm^2 and isolated single-crystal grains were grown with lateral size above 350 μm. When transferred onto Si/SiO_2 substrates, the grains showed field-effect mobility beyond 1300 cm^2/Vs. Our results provide a step closer towards an affordable commercialization of electronic-grade, large-area graphene.

KEYWORDS (graphene growth, chemical vapor deposition, isolated crystals, pre-oxidized copper, 2D materials, ethanol).

1. Introduction

Due to abundance, atomic lightness, bond strength and flexible hybridization, carbon allotropes are deemed fundamental building blocks for various advanced materials, which are key in many technologic fields. Among carbon allotropes, graphene, the basal plane of graphite, is the two dimensional (2D) material which was firstly isolated and studied [1]. The exceptionally high carrier mobility observed in exfoliated graphene samples (derived from mined graphite) [2–5] lured researchers to conceive the field of 2D electronics. The promised impact of such novel field is still to come, due to current technologic limitation in the production and processing of 2D materials.

The superior electrical properties of graphene are normally achieved in single-crystal exfoliated graphene, but it has proven hard to match those properties in large-area samples produced by even the most advanced technique – chemical vapor deposition (CVD). Samples are typically made of polycrystalline graphene, and the presence of grain boundaries are known to have a negative impact on graphene's physical properties, such as mobility, electron conductivity, and mechanical strength [6–8]. For this reason, an extensive effort was devoted to suppress the formation of grain boundaries and increase the size of graphene grains, mainly by decreasing the nucleation density. If a few graphene *nuclei* are widely spaced, they can grow as isolated single crystals and eventually merge into a continuous graphene film with reduced grain boundaries. Alternatively, all graphene *nuclei* were reported to grow with the same crystalline orientation on hydrogen-terminated Ge substrates [9]: Being them epitaxially correlated on an identically-oriented surface, they grow aligned along the same crystalline direction and ultimately merge into a single-crystal film without grain boundaries. However, this approach is still out of reach in the case of a polycrystalline Cu foil substrate, which is widely used for graphene growth due to a low price combined with a high graphene quality. In this case (growth on Cu via CVD of methane), the nucleation density was initially in the order of $\sim 10^6$ nuclei/cm^2 [10]. To minimize this high nucleation density, the CVD parameters were finely modulated by using high temperature (1000 ~ 1077 °C, close to the melting point of Cu (1084 °C)) [11–13], low precursor partial pressure [12,14], and high hydrogen-to-methane ratio [10,11,15,16]. To further control the nucleation sites, the Cu substrates were pre-treated by thermal annealing [17,18], electrochemical polishing [19], and pre-oxidation [17,20,21]. These efforts finally enabled the growth of millimeter-sized graphene grains [10,18].

Methane gas has been so far the preferential carbon source for the CVD growth of graphene on Cu. Being an efficient carbon precursor, ethanol can be used instead of methane and provide

various advantages. Being liquid at normal temperature and pressure, ethanol is safer than methane and can decompose at a lower temperature, accelerating the growth [22,23]. Continuous graphene films were grown on Cu foils at low partial pressures of ethanol (< 2 Pa) in seconds *i.e.,* much faster than conventional growth times (in the order of minutes) of methane-based CVD processes [20,24–27]. Shorter growth times are crucial for industrial production and can also limit growth kinetic issues related to Cu sublimation [28], which is also known to pollute the internal furnace walls during the CVD process, limiting the throughput [29]. Such an extremely fast growth of graphene occurs with an ethanol vapor flow as small as 0.1 sccm, one order of magnitude lower than those typical for methane. It is then challenging to increase the size of individual graphene grains above 5 μm without a specific strategy aimed at limiting the nucleation density [30]. The pre-oxidation of the Cu foils is an effective way for reducing the number of nucleation sites and obtain large single-crystal graphene samples [10,18,21,27,31–33]. By pre-oxidizing the Cu foils at 250 °C, the nucleation density became as low as ~ 1 nucleus/cm^2, five orders of magnitude smaller than that reported for untreated Cu foils [18,27,31–34]. When the Cu foil is covered by an oxide layer, its surface is passivated and the presence of impurities acting as nucleation seeds is abated [10,17,21,35–38]. However, it should be noted that an unwanted amount of oxygen is often uncontrollably introduced into the CVD chamber for several potential reasons: i) imperfect vacuum sealing, ii) use of hydrolyzers for the production of H_2 gas [39]. Other than the presence of residual oxygen, the different quality and processing of Cu foils, depending on the production process (cold-rolled or soft-annealed) and the degree of purity (oxygen-free or oxygen-rich) [21,40–46] are associated with a confirmed difficulty to reproduce results.

Most of the recent studies on the growth of large single crystal graphene covered the CVD of methane [12], while ethanol as a carbon source has not been investigated in this respect yet. Up to

date, only one group reported the growth of mm-sized single crystal graphene by CVD of ethanol with pre-oxidized Cu "enclosures" [27]. The enclosure approach is not ideal because it introduces uncertainties to the CVD process: It is impossible to define the gaseous environment inside the enclosure's internal surfaces. If the enclosures are physically sealed and gas-tight, then carbon would be either present as a contaminant on the copper surface, or it would diffuse inside across the Cu foils bulk, possibly along grain boundaries [21]. Instead, if the enclosures are not perfectly sealed, then the precursors could flow in and out, along the uncertain "pliers-crimped edges". In this framework, it is crucial to optimize the early nucleation stages on a flat Cu surface directly exposed to the gas atmosphere. In this work, we demonstrate the CVD growth of isolated graphene grains larger than 350 μm by using ethanol and pre-oxidized flat Cu foils. By using low pressure (130 - 400 Pa) and small ethanol flow (1.5×10^{-3} sccm), the nucleation site density was considerably reduced. Overall, we abated the nucleation density to 3 nuclei/mm^2 and tuned the CVD parameters to control the growth process for a time long enough (an hour) to produce sub-mm graphene grains with high crystallinity and few defects. The synthesized graphene islands are single-crystal with field-effect mobility beyond 1300 cm^2/Vs, demonstrating the potential of our growth method for the fabrication of high performance graphene electronic devices.

2. Experimental

2.1 Sample preparation

As previously reported, the CVD system was made of a quartz tube vessel, coaxial to a tube furnace [25,47,48], which was modified with inner screens of alumina and tantalum to avoid the issue of quartz contamination [29]. Cu foils (SE Cu 58, cold worked Oxygen Free Copper 99.95%), cut into 2x2 cm substrates, were washed in a cycle of ultrasonic baths (5 min each in acetone and ethanol). For the pre-oxidation treatment, the Cu substrates were heated on a hot plate at 250°C in

air (from 0 to 150 min as reported, with ramping rate of 8 °C/min). Then Cu substrates were slowly cooled down to room temperature to prevent the formation of micro-cracks in the copper oxide layer, which could expose bare metal. The oxidized Cu substrates were inserted inside the reactor vessel under controlled pressure, and quickly moved from the room-temperature zone into the hot zone without breaking the vacuum when the growth temperature was reached. During the growth phase H_2, Ar (20sccm) and ethanol vapor were supplied. The H_2 and ethanol vapor flows ranged between 10-100 sccm and 1.5×10^{-3}-0.1 sccm, respectively. Before the introduction of ethanol vapors in the chamber, the Cu substrates were thermalized in Ar atmosphere (20 sccm) at the same growth temperature for a given annealing time (1-20 min). The growth time was defined between the onset of the precursor flow and the extraction of the sample from the hot zone. Ethanol vapor was fed with Ar carrier gas by using a pressurized bubbler kept at 0°C in an iced water bath, so that the partial pressure of ethanol was 15 mbar (1.5×10^3 Pa) in 3 bar (3×10^4 Pa) Ar. When the Cu substrates were extracted from the hot zone, they were cooled down to room temperature in Ar atmosphere (750 sccm). Other details on the CVD apparatus and the growth procedure were reported in previous work by the group [29].

2.2 *Sample characterization*

To optically visualize the growth of isolated graphene grains, the Cu substrates were heated in air on a hot plate at 180 °C for 30 min [21]: The uncovered Cu regions were mildly oxidized, providing color contrast with those under the graphene grains which retained the metallic luster. For further characterization, the samples were also transferred on SiO_2/Si substrate using cyclododecane transfer method [47,49].

Raman scattering measurements were carried out with a HORIBA Scientific LabRAM HR Evolution Raman spectrometer with an integrated Olympus BX41 microscope and 532 nm laser.

Low laser power of < 1 mW minimized degradation or damages of graphene. The morphology was characterized by tapping-mode atomic force microscopy (AIST-NT SPM AFM) and scanning electron microscopy (SEM, FEG FEI Helios NanoLab 600i).

2.3 *Field-effect transistors fabrication and electrical measurements*

The graphene samples on Si/SiO_2 substrate were patterned by e-beam lithography and etched by oxygen plasma to define the graphene channels, and sequentially annealed at 345 ℃ for 3 h in a mixture of Ar (95%) and H_2 (5%) to remove residues from graphene. Metal electrodes were patterned by e-beam lithography and Cr/Pd/ Au (1/30/40 nm) metals were deposited by e-beam evaporator. Electrical measurements were taken with a semiconductor parameter analyzer (Keithley 2400) in ambient condition.

3. Results and discussion

The graphene growth by ethanol is so efficient and rapid that a continuous polycrystalline film can grow in few seconds, even less than 60 [26]. With ethanol flow rate Q_{eth} = 0.1 sccm, a continuous film grew in 15 s (Figure 1a). The Raman analysis in Figure 1b-d shows that the graphene is monolayer ($I_{2D}/I_G \sim 2.7$) and slightly defective ($A_D/A_G \cong 0.5$). To decrease the nucleation density and obtain isolated graphene grains, the growth rate was tuned by setting $Q_{eth} = 1.5\times10^{-2}$ sccm. In these conditions, individual graphene grains grew with 1-3 μm size (Figure 1e). These grains are made of monolayer graphene ($I_{2D}/I_G \cong 2.3$) with lower defect density ($A_D/A_G \cong 0.3$) than the continuous film. The morphology of the islands was further investigated AFM (Figure 1i-l). The Cu foil substrates (polycrystalline) underwent substantial recrystallization during the CVD processes. AFM images taken on the Cu substrates indicate that the graphene island do not have a distinctive polygonal shape; however, hexagonal islands fully cover specific Cu grains, possibly

those with Cu (111) facets [50]. It is expected that single-crystal graphene grains might become more regular as the precursor flow is lowered and the growth rate is reduced [50].

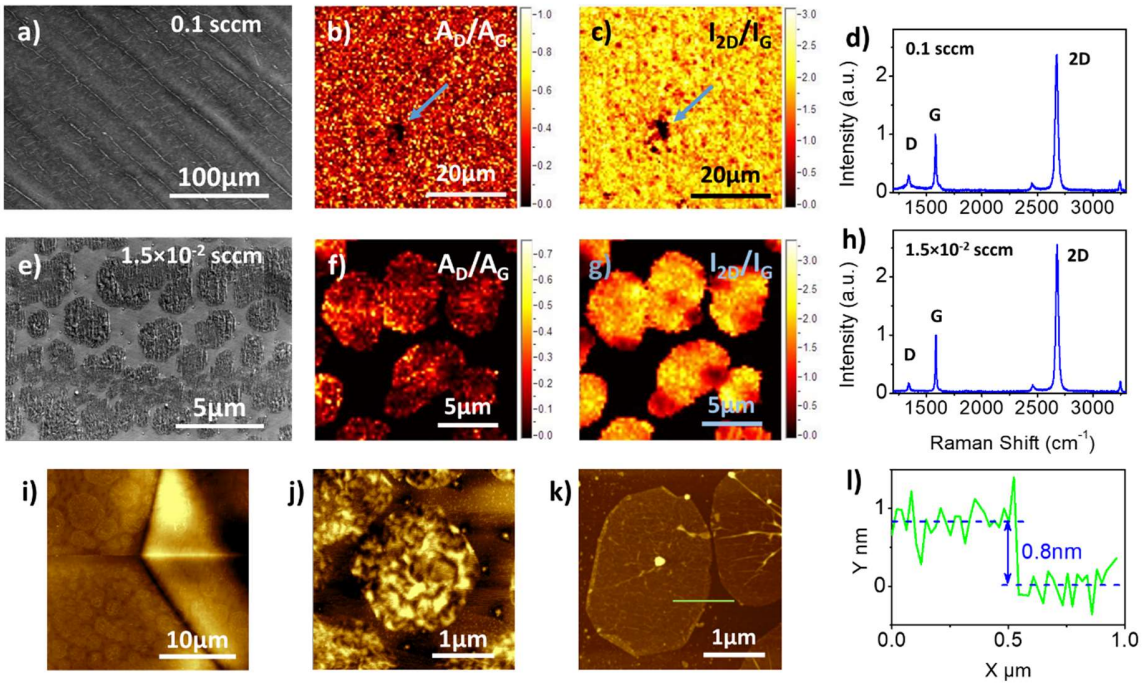

Figure 1. Graphene grown for 15 s with (a-d) Q_{eth} = 0.1 sccm and (e-h) Q_{eth} = 1.5×10^{-2} sccm. (a,e) SEM micrographs of the graphene on the Cu substrates. (b,c) Raman mapping images (50 x 50 µm in size, 0.5 µm resolution) for A_D/A_G (peak integrated area ratio) and I_{2D}/I_G (peak intensity ratio) after transfer on SiO_2/Si. The blue arrow indicates a small tear caused by transfer. f,g) Raman mapping images (17 x 17 µm in size, 0.25 µm resolution) for A_D/A_G and I_{2D}/I_G of graphene islands after transfer on SiO_2/Si. The sample is composed of isolated monolayer graphene grains of 1 - 3 µm with smaller disorder level. (d,h) Representative (averaged) Raman spectra. (i-l) AFM analysis of graphene grown with Q_{eth} = 1.5×10^{-2} sccm. (i) Graphene grains on Cu foil; the differences in shapes are related to the Cu facets where the grains are grown. (j) High-resolution AFM image of single grains (on Cu) with hexagonal shape. (k) AFM image after transfer on

SiO_2/Si with l) height profile (showing a step of 0.8 nm). Some wrinkles due to the transfer process appear.

To obtain regular grains with sizes beyond a few microns, we applied a pre-oxidation treatment to the Cu substrates and investigated the effect of the pre-oxidation time on the nucleation density (δ_n). As pre-oxidation treatment, the Cu foils were annealed in air at 250 °C for a time (t_{ox}) ranging from 0 to 150 min (Figure 2).

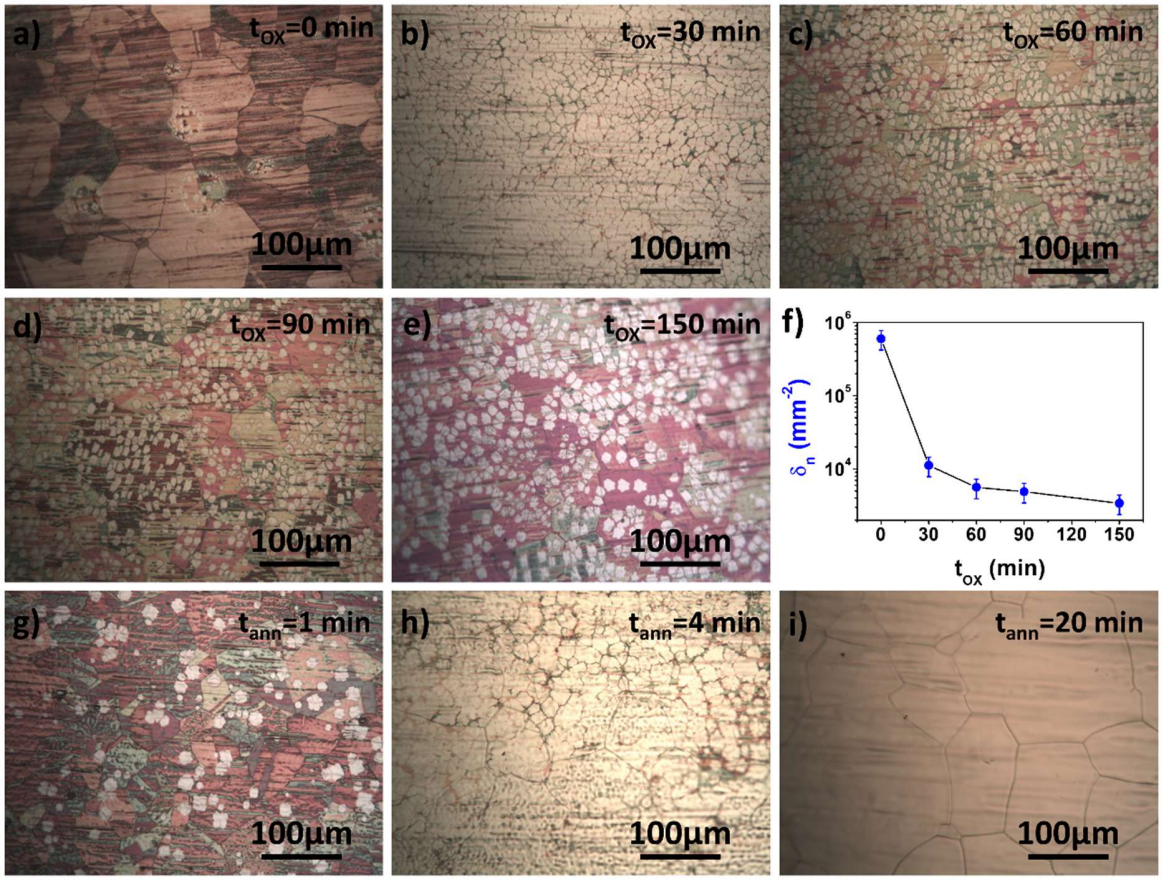

Figure 2. Nucleation density of graphene grown on Cu substrate with different pre-oxidation (250°C in air) time (t_{OX}) ranging from 0 to 150 min. (a-e) Optical microscopy of the graphene grown on Cu in the various cases. (f) Nucleation density trend *vs* pre-oxidation time. (g-i) Nucleation density of graphene grown on pre-oxidized Cu substrate (250°C in air for 150min) with

different pre-growth Ar annealing times (t_{ann}). Isolated grains grew only with 1 min Ar annealing, while in the other cases continuous films grew.

With no pre-oxidation (t_{ox} = 0 min), the $\delta_n = 6\times10^5$ nuclei/mm^2 (Figure 3a). For t_{ox} = 30 min, the nucleation density drastically decrease ($\delta_n = 1.1\times10^4$ nuclei/mm^2). At longer times, δ_n keeps on slightly decreasing, reaching $\delta_n = 3.4\times10^3$ nuclei/mm^2 at t_{ox} = 150 min: Such nucleation density is more than two orders of magnitude smaller than the value obtained on non-oxidized Cu. The grains' growth rate is ~0.08 μm/s and they reached an average size of ~20 μm (Figure 2e). Having set the duration of the pre-oxidation treatment to 150 min, we investigated the effect of the Ar annealing on the growth (Figure 2g-i). The Ar annealing was done in vacuum just before the CVD growth in the furnace. By varying the Ar annealing time from 1 to 20 min, we discovered that such pre-oxidation treatment was effective in reducing the nucleation density only with an Ar annealing of 1 min before the CVD growth. With a Ar annealing time longer than 1 min. the effect of the pre-oxidation on the nucleation suppression was cancelled and continuous graphene resumed growing. The combined effect of pre-oxidation and Ar annealing can be explained in terms of copper reconstruction and sublimation [28]. During the pre-oxidation treatment, both cupric oxide (CuO) and cuprous oxide (Cu_2O) are formed on the Cu surface [27]. At AFM analysis, the pre-oxidized Cu surface appears highly roughened due to typical clusters of sub-μm Cu oxide spheroids (not shown) [51]. The Ar annealing rids the Cu surface of oxides in a few seconds (as predicted by the Cu/O_2 phase diagram [52]); this should restore the catalytic activity of metallic Cu, but the reconstructed surface is very smooth and offers fewer nucleation sites, such as defects and carbon contaminations, than the original Cu foil [28, 53]. When the Ar annealing lasts for longer times (t_{ann} > 1 min), the intense Cu sublimation and re-deposition induce new nucleation sites and thus the growth of continues films resumes [28]. After determining the initial conditions

for the growth of individual grains (Cu pre-oxidation at 250°C in air for 150 min, Ar annealing in vacuum for 1 min), the CVD parameters were optimized to obtain crystalline graphene grain of sub-mm size. The process steps are reported in Table 1.

Table 1. Optimization of the CVD conditions to make large-area, single-crystal graphene grains via ethanol-CVD on pre-oxidized, flat Cu substrates.

Process	T (°C)	Time (s)	P (Pa)	Q_{eth} (sccm)	H_2 (sccm)	A_D/A_G	I_{2D}/I_G	δ_n (nuclei/mm^2)	Size (μm)
P1	1000	1800	130	1.5×10^{-2}	100	0.6±0.1	2.4±0.1	3.7×10^{2}	40±12
P2	1000	1800	130	1.5×10^{-3}	100	0.3±0.1	2.4±0.3	3	45.4±5.5
P3	1070	1800	130	1.5×10^{-3}	10	0.3±0.1	2.5±0.2	<3	90.3±8.9
P4	1070	1800	400	1.5×10^{-3}	10	0.2±0.1	2.5±0.4	<3	216.0±20.2
P5	1070	3600	400	1.5×10^{-3}	10	0.1±0.1	2.4±0.1	<3	359.6±75.3

At first, the effect of the ethanol flow on the grain size was further investigated by comparing the growth at 1.5×10^{-2} and 1.5×10^{-3} sccm. By decreasing the flow, the nucleation density turned from 3.7×10^{2} (P1, Figure 3a) to δ_n = 3 nuclei/mm^2 (P2, Figure 3b). In the latter case, monolayer grains ($I_{2D}/I_G \approx 2.4$) grew larger than 40 μm and with low defect density (A_D/A_G from 0.6 to 0.3). The use of a smaller ethanol flow on oxidized Cu successfully decelerated the growth rate and favored the appearance of grains with regular and well-defined shape [12].

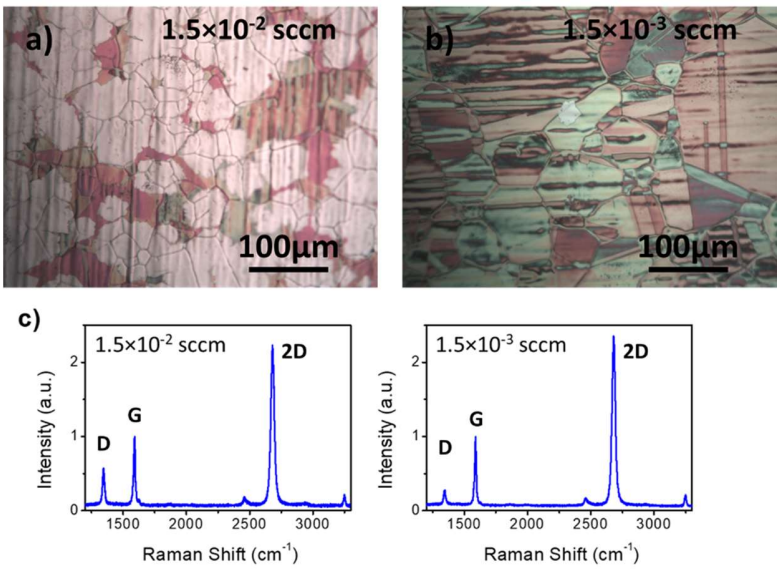

Figure 3. Optical images of graphene (30 min, 1000° C, 130 Pa) grown on pre-oxidized Cu foil with (a) 1.5×10^{-2} sccm (P1) and (b) 1.5×10^{-3} sccm of ethanol (P2). c) Corresponding Raman spectra.

A detailed characterization of one 50-µm grain (130 Pa and 1.5×10^{-3} sccm) was carried out by AFM and Raman mapping (Figure 4). In line with Figure 3c, the Raman map (Figure 4c) shows $A_D/A_G < 0.2$, with peak values of ~ 0.3 on small regions affected by the transfer process. The I_{2D}/I_G map (mean value of ~ 2.4, Figure 4d) also confirms the overall uniformity of the grain. The grain measured by AFM has a step of ~ 1 nm (Figure 4b), compatible with the monolayer thickness previously inferred by Raman spectroscopy.

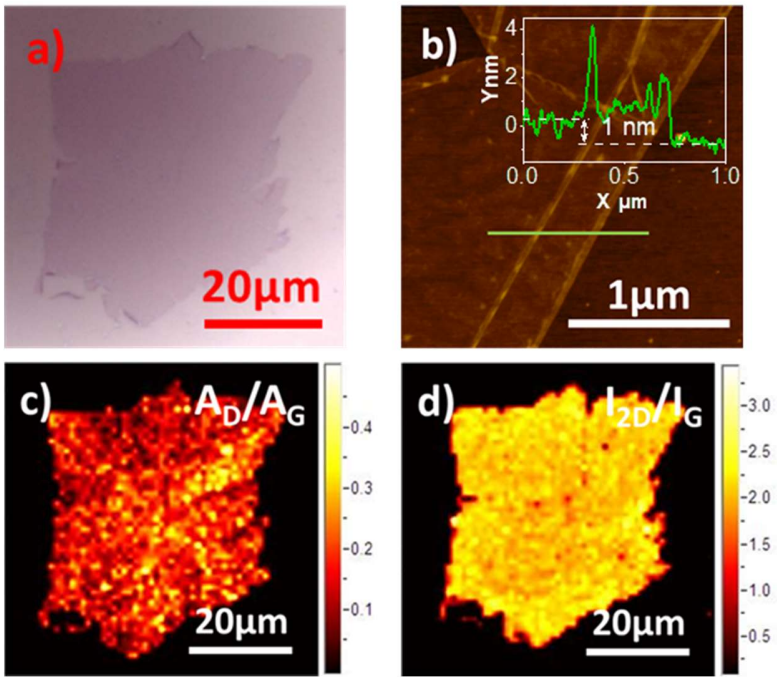

Figure 4. Analysis of a 50-µm grain (sample P2) after transfer onto Si/SiO_2. (a) Optical micrograph of the grain, (b) AFM topography image with thickness line profile of ~ 1 nm. The value is larger than the inter-plane spacing of graphite (0.335 nm) due to intercalated molecules and to the interaction forces between graphene-substrate-tip, as found for CVD-graphene in similar experimental and environmental (relative humidity) conditions [51–53]. Raman mapping images of (b) A_D/A_G and (c) I_{2D}/I_G peak ratio (60 µm × 60 µm area, 0.5 µm spatial resolution).

After setting the ethanol flow to 1.5×10^{-3} sccm, the CVD temperature was raised from 1000°C to 1070°C, to fully exploit the fast growth kinetics granted by ethanol aiming at increasing the grain size and crystallinity (Figure 5). At 1070 °C, single-crystal grain reached sizes over 90 µm (P3, Figure 5a). Raman analysis shows $I_{2D}/I_G = 2.5$ and $A_D/A_G = 0.3$, a typical Raman signature of crystalline monolayer graphene, with lower defect level than at 1000°C (Figure 5d). By raising the gas total pressure (400 Pa) during the growth, the graphene grains extended their sizes to more than 200 µm (P4, Figure 5b). In these conditions, by bringing the growth time to 60 min, sub-mm

grains (larger than 350 µm) grew with regular geometric shape and sharply defined edges (P5, Figure 5c). The Raman spectra in Figure 5d shows $I_{2D}/I_G = 2.5$ [54,55] and $A_D/A_G < 0.1$. Graphene grown for 60 min showed the lowest defect related D peak intensity, which was probably induced by the transfer process because no D peak was observed in as-grown graphene on Cu substrate (Figure S1).

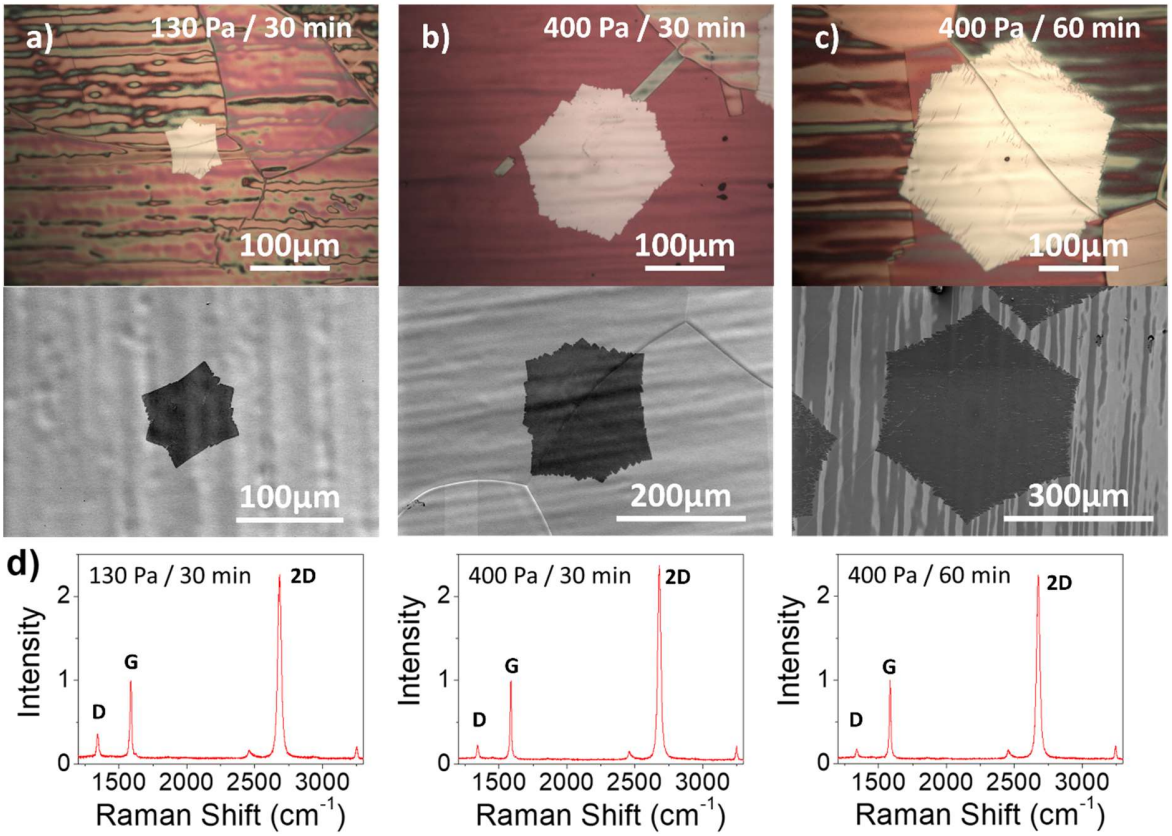

Figure 5. Optical and SEM images of the single-crystal graphene grains grown at 1070 °C with 1.5×10^{-3} sccm of ethanol: (a) 130 Pa, 30 min (P3); (b) 400 Pa, 30 min (P4); (c) 400Pa, 60 min (P5). (d) Raman spectra of the samples transferred onto Si/SiO_2.

Figure 6a shows the edge morphology of a graphene grain (P5, 350 µm in size) on Cu substrate. The thickness measured by AFM is ~ 1 nm, compatible with monolayer graphene on Si/SiO_2 (Figure 6b). Raman mapping images (50 × 50 µm) acquired on the grain edge highlight the

uniformity of the sample, with $A_D/A_G \leq 0.1$ (Figure 6c). Small regions with $A_D/A_G > 0.2$ correspond to minor contaminations, wrinkles and folds due to transfer process. The Raman peak ratio $I_{2D}/I_G > 2$ confirms the monolayer thickness (Figure 6d).

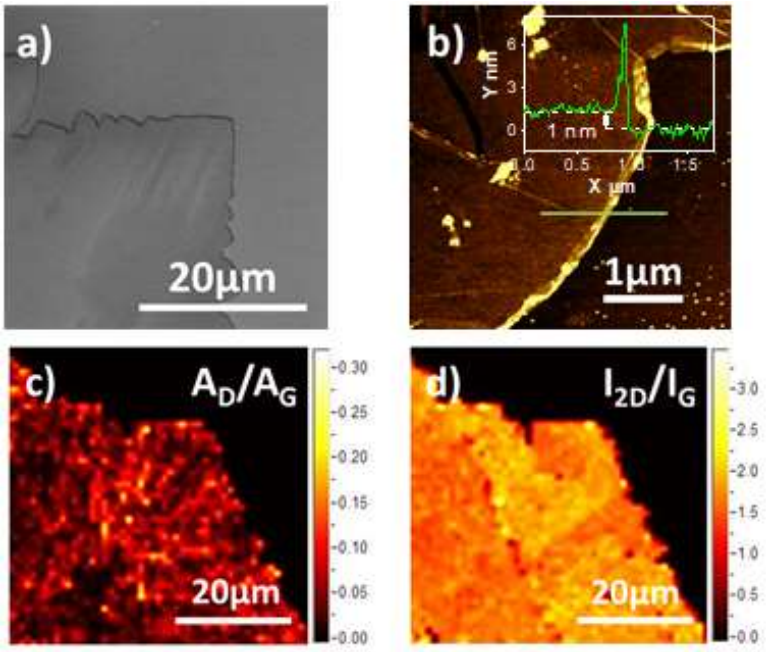

Figure 6. Analysis of a 350-µm graphene grain (P5: 1.5×10^{-3} sccm ethanol, 1070° C, 130 Pa, 60 min). (a) SEM image and (b) AFM topography image with thickness line profile of the grain edge. Raman mapping images of (c) A_D/A_G and (d) I_{2D}/I_G.

To summarize, the optimization steps led to a concurrent decrease in nucleation density and to a major increase in grain size, as reported in Figure 7. The successful growth of large single-crystal graphene by ethanol-CVD might be possibly attributed to oxygen atoms dissociated from ethanol, which would act as nucleation inhibitors by suppressing the formation of new nucleation sites [21]. However, in ethanol-CVD, oxygen might also act as a growth enhancer promoting the quick growth of graphene on a Cu substrate [26]. Therefore, this growth platform would deserve further investigations in order to fully understand the overall effect of oxygen on the nucleation and growth of graphene.

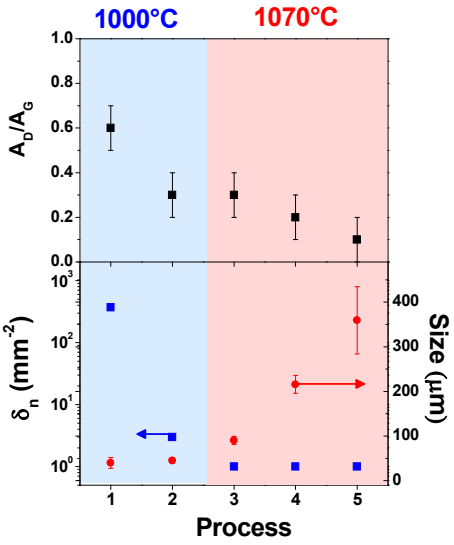

Figure 7. Optimization steps performed to reduce nucleation density δ_n according to Table 1. Grain size and A_D/A_G are also reported.

To investigate electrical properties of the large grains (P5), we fabricated devices with transmission line method (TLM) geometry, as shown in Figure 8a. Figure 8b shows transfer curve (I_D-V_G) of a representative graphene device. The charge neutral point is shifted to ~ 50 V, indicating that graphene is highly p-doped. The p-doping behavior of graphene can be caused by various extrinsic factors, such as residues from the wet-transfer process, charged impurities on the SiO_2 substrate, and trapped molecule between graphene channel and substrate [56,57]. The inset shows linear output curves (I_D-V_D) with gate voltage dependence, demonstrating Ohmic contact between graphene and metal electrodes.

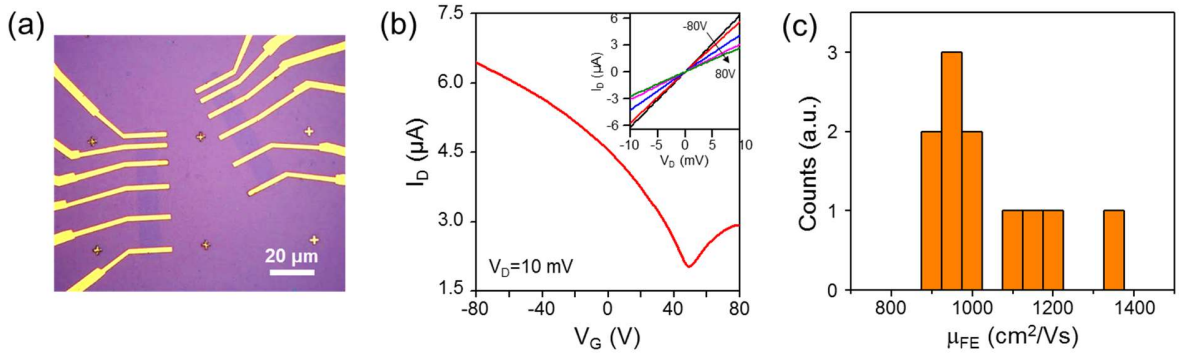

Figure 8. (a) Optical image of graphene devices with TLM geometry. (b) Transfer curve (I_D-V_G) of a representative graphene device. The inset shows the output curves (I_D-V_D) at different gate voltages. (c) Histogram of field-effect mobilities measured from eleven graphene devices.

The field-effect mobility (μ_{FE}) of graphene was calculated by using the equation,

$$\mu_{FE} = \frac{L}{WC_iV_D}\left(\frac{dI_D}{dV_G}\right)$$

where L, W and C_i are channel length, width and capacitance of SiO_2, respectively. As shown in Figure 8c, the extracted filed-effect mobility ranges from 912 to 1355 cm^2/Vs. These mobility values are generally lower than those reported for continuous, monolayer graphene grown on Cu (not pre-oxidized) by methane-CVD [31,58], but are comparable to [24] or higher than the values of polycrystalline graphene films grown on Cu (not pre-oxidized) by alcohol-type precursors [59]. In the case of isolated grains (transferred onto Si/SiO_2), to date a few works reported higher mobility values for methane-CVD growth [11,46,60–62], but no one ever disclosed mobility values of ethanol-grown grains [27,63]. We further calculated sheet resistances (R_{sh}) of the graphene grains at V_G = 0 V (no electrical doping): The best samples attained a sheet resistance of 550-610 Ω/□, highlighting the potential of ethanol-grown graphene as a transparent conducting material.

Conclusion

We demonstrated the growth of sub-mm, highly crystalline monolayer graphene grains by CVD of ethanol on flat Cu foils, without the need of using Cu enclosures or other artifices to limit the nucleation density. Our study systematically explored the ethanol-CVD parameters to afford the growth of graphene on flat Cu foils with full control over nucleation rate, grain size and crystallinity. Without Cu pre-oxidation, the high nucleation density granted by ethanol-CVD prevented the growth of grains larger than 1-3 μm. By using Cu pre-oxidation, we optimized the growth process by tuning the CVD parameters. A combination of Cu pre-oxidation, quick Ar annealing (1 min, pre-growth) and low ethanol flow rate (1.5×10^{-3} sccm) are the key to the growth of isolated large graphene grains on plain Cu with size in excess of 300 μm. When used in field-effect transistors, these large grains attained field-effect mobility up to 1355 cm^2/Vs. With these optimized CVD conditions, a few nucleation sites were formed and the carbon atoms dissociated from ethanol were preferentially incorporated into the growing *nuclei* instead of further contributing to the nucleation. With these conditions, the growth process could be extended to 60 min to increase the grain size while retaining a low nucleation density. Overall, the growth of sub-mm single-crystal grains with low defects on flat Cu surfaces is very significant for technologic applications. Having a reproducible production method, these crystalline grains can be made in large numbers to be used as building blocks for electronic devices. Further, crystalline grains as such could serve as seeds for the formation of continuous large-area, single-crystal graphene films, which are actively sought after in the materials community.

ACKNOWLEDGMENT

A.C. is supported by the Yonsei University Research Fund (Yonsei Frontier Lab. Young Researcher Supporting Program) of 2018. G.H.L is supported by the International Research & Development Program of the National Research Foundation of Korea (NRF) funded by the Ministry of Education, Science and Technology (MEST) of Korea (NRF-2016K1A3A1A25003573), Basic Science Research Program through the National Research Foundation of Korea (NRF) funded by the Ministry of Science, ICT & Future Planning (2017R1A5A1014862, SRC program: vdWMRC center), and the Korea Institute of Energy Technology Evaluation and Planning(KETEP) and the Ministry of Trade, Industry & Energy(MOTIE) of the Republic of Korea (No. 20173010013340).

REFERENCES

(1) Novoselov, K. S.; Geim, A. K.; Morozov, S. V; Jiang, D.; Zhang, Y.; Dubonos, S. V; Grigorieva, I. V; Firsov, A. A. Electric Field Effect in Atomically Thin Carbon Films. *Science (80-.).* **2004**, *306* (5696), 666–669.

(2) Bolotin, K. I.; Sikes, K. J.; Jiang, Z.; Klima, M.; Fudenberg, G.; Hone, J.; Kim, P.; Stormer, H. L. Ultrahigh Electron Mobility in Suspended Graphene. *Solid State Commun.* **2008**, *146* (9), 351–355. https://doi.org/https://doi.org/10.1016/j.ssc.2008.02.024.

(3) Morozov, S. V; Novoselov, K. S.; Katsnelson, M. I.; Schedin, F.; Elias, D. C.; Jaszczak, J. A.; Geim, A. K. Giant Intrinsic Carrier Mobilities in Graphene and Its Bilayer. *Phys. Rev. Lett.* **2008**, *100* (1), 16602. https://doi.org/10.1103/PhysRevLett.100.016602.

(4) Geim, A. K.; Novoselov, K. S. The Rise of Graphene. *Nat. Mater.* **2007**, *6*, 183.

(5) Du, X.; Skachko, I.; Barker, A.; Andrei, E. Y. Approaching Ballistic Transport in Suspended Graphene. *Nat. Nanotechnol.* **2008**, *3*, 491.

(6) Ogawa, Y.; Komatsu, K.; Kawahara, K.; Tsuji, M.; Tsukagoshi, K.; Ago, H. Structure and Transport Properties of the Interface between CVD-Grown Graphene Domains. *Nanoscale* **2014**, *6* (13), 7288–7294. https://doi.org/10.1039/C3NR06828E.

(7) Ago, H.; Fukamachi, S.; Endo, H.; Solís-Fernández, P.; Mohamad Yunus, R.; Uchida, Y.; Panchal, V.; Kazakova, O.; Tsuji, M. Visualization of Grain Structure and Boundaries of Polycrystalline Graphene and Two-Dimensional Materials by Epitaxial Growth of Transition Metal Dichalcogenides. *ACS Nano* **2016**, *10* (3), 3233–3240. https://doi.org/10.1021/acsnano.5b05879.

(8) Huang, P. Y.; Ruiz-Vargas, C. S.; van der Zande, A. M.; Whitney, W. S.; Levendorf, M. P.; Kevek, J. W.; Garg, S.; Alden, J. S.; Hustedt, C. J.; Zhu, Y.; et al. Grains and Grain Boundaries in Single-Layer Graphene Atomic Patchwork Quilts. *Nature* **2011**, *469* (7330), 389–392.

(9) Lee, J.-H.; Lee, E. K.; Joo, W.-J.; Jang, Y.; Kim, B.-S.; Lim, J. Y.; Choi, S.-H.; Ahn, S. J.; Ahn, J. R.; Park, M.-H.; et al. Wafer-Scale Growth of Single-Crystal Monolayer Graphene on Reusable Hydrogen-Terminated Germanium. *Science (80-.).* **2014**, *344* (6181), 286–289.

(10) Zhou, H.; Yu, W. J.; Liu, L.; Cheng, R.; Chen, Y.; Huang, X.; Liu, Y.; Wang, Y.; Huang, Y.; Duan, X. Chemical Vapour Deposition Growth of Large Single Crystals of Monolayer and Bilayer Graphene. *Nat. Commun.* **2013**, *4*, 2096. https://doi.org/10.1038/ncomms3096.

(11) Yan, Z.; Lin, J.; Peng, Z.; Sun, Z.; Zhu, Y.; Li, L.; Xiang, C.; Samuel, E. L.; Kittrell, C.; Tour, J. M. Toward the Synthesis of Wafer-Scale Single-Crystal Graphene on Copper Foils. *ACS Nano* **2012**, *6* (10), 9110–9117. https://doi.org/10.1021/nn303352k.

(12) Li, X.; Magnuson, C. W.; Venugopal, A.; An, J.; Suk, J. W.; Han, B.; Borysiak, M.; Cai, W.; Velamakanni, A.; Zhu, Y.; et al. Graphene Films with Large Domain Size by a Two-Step Chemical Vapor Deposition Process. *Nano Lett.* **2010**, *10* (11), 4328–4334. https://doi.org/10.1021/nl101629g.

(13) Kim, H.; Mattevi, C.; Calvo, M. R.; Oberg, J. C.; Artiglia, L.; Agnoli, S.; Hirjibehedin, C. F.; Chhowalla, M.; Saiz, E. Activation Energy Paths for Graphene Nucleation and Growth on Cu. *ACS Nano* **2012**, *6* (4), 3614–3623. https://doi.org/10.1021/nn3008965.

(14) Zhang, Y. H.; Chen, Z. Y.; Wang, B.; Wu, Y. W.; Jin, Z.; Liu, X.; Yu, G. H. *Controllable Growth of Millimeter-Size Graphene Domains on Cufoil*; 2013; Vol. 96. https://doi.org/10.1016/j.matlet.2013.01.024.

(15) Mohsin, A.; Liu, L.; Liu, P.; Deng, W.; Ivanov, I. N.; Li, G.; Dyck, O. E.; Duscher, G.; Dunlap, J. R.; Xiao, K.; et al. Synthesis of Millimeter-Size Hexagon-Shaped Graphene Single Crystals on Resolidified Copper. *ACS Nano* **2013**, *7* (10), 8924–8931. https://doi.org/10.1021/nn4034019.

(16) Jacobberger, R. M.; Arnold, M. S. Graphene Growth Dynamics on Epitaxial Copper Thin Films. *Chem. Mater.* **2013**, *25* (6), 871–877. https://doi.org/10.1021/cm303445s.

(17) Eres, G.; Regmi, M.; Rouleau, C. M.; Chen, J.; Ivanov, I. N.; Puretzky, A. A.; Geohegan, D. B. Cooperative Island Growth of Large-Area Single-Crystal Graphene on Copper Using Chemical Vapor Deposition. *ACS Nano* **2014**, *8* (6), 5657–5669. https://doi.org/10.1021/nn500209d.

(18) Gan, L.; Luo, Z. Turning off Hydrogen To Realize Seeded Growth of Subcentimeter Single-Crystal Graphene Grains on Copper. *ACS Nano* **2013**, *7* (10), 9480–9488. https://doi.org/10.1021/nn404393b.

(19) Luo, Z.; Lu, Y.; Singer, D. W.; Berck, M. E.; Somers, L. A.; Goldsmith, B. R.; Johnson, A. T. C. Effect of Substrate Roughness and Feedstock Concentration on Growth of Wafer-Scale Graphene at Atmospheric Pressure. *Chem. Mater.* **2011**, *23* (6), 1441–1447. https://doi.org/10.1021/cm1028854.

(20) Li, X.; Magnuson, C. W.; Venugopal, A.; Tromp, R. M.; Hannon, J. B.; Vogel, E. M.;

Colombo, L.; Ruoff, R. S. Large-Area Graphene Single Crystals Grown by Low-Pressure Chemical Vapor Deposition of Methane on Copper. *J. Am. Chem. Soc.* **2011**, *133* (9), 2816–2819. https://doi.org/10.1021/ja109793s.

(21) Hao, Y.; Bharathi, M. S.; Wang, L.; Liu, Y.; Chen, H.; Nie, S.; Wang, X.; Chou, H.; Tan, C.; Fallahazad, B.; et al. The Role of Surface Oxygen in the Growth of Large Single-Crystal Graphene on Copper. *Science (80-.).* **2013**, *342* (6159), 720 LP-- 723.

(22) Capasso, A.; Dikonimos, T.; Sarto, F.; Tamburrano, A.; De Bellis, G.; Sarto, M. S.; Faggio, G.; Malara, A.; Messina, G.; Lisi, N. Nitrogen-Doped Graphene Films from Chemical Vapor Deposition of Pyridine: Influence of Process Parameters on the Electrical and Optical Properties. *Beilstein J. Nanotechnol.* **2015**, *6*, 2028–2038. https://doi.org/10.3762/bjnano.6.206.

(23) Capasso, A.; Salamandra, L.; Faggio, G.; Dikonimos, T.; Buonocore, F.; Morandi, V.; Ortolani, L.; Lisi, N. Chemical Vapor Deposited Graphene-Based Derivative As High-Performance Hole Transport Material for Organic Photovoltaics. *ACS Appl. Mater. Interfaces* **2016**, *8* (36), 23844–23853. https://doi.org/10.1021/acsami.6b06749.

(24) Guermoune, A.; Chari, T.; Popescu, F.; Sabri, S. S.; Guillemette, J.; Skulason, H. S.; Szkopek, T.; Siaj, M. Chemical Vapor Deposition Synthesis of Graphene on Copper with Methanol, Ethanol, and Propanol Precursors. *Carbon N. Y.* **2011**, *49* (13), 4204–4210. https://doi.org/http://dx.doi.org/10.1016/j.carbon.2011.05.054.

(25) Faggio, G.; Capasso, A.; Messina, G.; Santangelo, S.; Dikonimos, T.; Gagliardi, S.; Giorgi, R.; Morandi, V.; Ortolani, L.; Lisi, N. High-Temperature Growth of Graphene Films on Copper Foils by Ethanol Chemical Vapor Deposition. *J. Phys. Chem. C* **2013**, *117* (41),

21569–21576. https://doi.org/10.1021/jp407013y.

(26) Lisi, N.; Buonocore, F.; Dikonimos, T.; Leoni, E.; Faggio, G.; Messina, G.; Morandi, V.; Ortolani, L.; Capasso, A. Rapid and Highly Efficient Growth of Graphene on Copper by Chemical Vapor Deposition of Ethanol. *Thin Solid Films* **2014**, *571*, 139–144. https://doi.org/http://dx.doi.org/10.1016/j.tsf.2014.09.040.

(27) Chen, X.; Zhao, P.; Xiang, R.; Kim, S.; Cha, J.; Chiashi, S.; Maruyama, S. Chemical Vapor Deposition Growth of 5mm Hexagonal Single-Crystal Graphene from Ethanol. *Carbon N. Y.* **2015**, *94*, 810–815. https://doi.org/http://dx.doi.org/10.1016/j.carbon.2015.07.045.

(28) Vlassiouk, I.; Smirnov, S.; Regmi, M.; Surwade, S. P.; Srivastava, N.; Feenstra, R.; Eres, G.; Parish, C.; Lavrik, N.; Datskos, P.; et al. Graphene Nucleation Density on Copper: Fundamental Role of Background Pressure. *J. Phys. Chem. C* **2013**, *117* (37), 18919–18926. https://doi.org/10.1021/jp4047648.

(29) Lisi, N.; Dikonimos, T.; Buonocore, F.; Pittori, M.; Mazzaro, R.; Rizzoli, R.; Marras, S.; Capasso, A. Contamination-Free Graphene by Chemical Vapor Deposition in Quartz Furnaces. *Sci. Rep.* **2017**, *7* (1), 9927. https://doi.org/10.1038/s41598-017-09811-z.

(30) SINGH, A. K.; GUPTA, A. K. Facet-Dependent Study of Efficient Growth of Graphene on Copper by Ethanol-CVD. *Bull. Mater. Sci.* **2015**, *38* (7), 1723–1729. https://doi.org/10.1007/s12034-015-1045-2.

(31) Miseikis, V.; Convertino, D.; Mishra, N.; Gemmi, M.; Mashoff, T.; Heun, S.; Haghighian, N.; Bisio, F.; Canepa, M.; Piazza, V.; et al. Rapid CVD Growth of Millimetre-Sized Single Crystal Graphene Using a Cold-Wall Reactor. *2D Mater.* **2015**, *2* (1), 14006.

https://doi.org/10.1088/2053-1583/2/1/014006.

(32) Li, J.; Wang, X.-Y.; Liu, X.-R.; Jin, Z.; Wang, D.; Wan, L.-J. Facile Growth of Centimeter-Sized Single-Crystal Graphene on Copper Foil at Atmospheric Pressure. *J. Mater. Chem. C* **2015**, *3* (15), 3530–3535. https://doi.org/10.1039/C5TC00235D.

(33) Suzuki, S.; Kiyosumi, K.; Nagamori, T.; Tanaka, K.; Yoshimura, M. Low Density Growth of Graphene by Air Introduction in Atmospheric Pressure Chemical Vapor Deposition. *e-Journal Surf. Sci. Nanotechnol.* **2015**, *13*, 404–409. https://doi.org/10.1380/ejssnt.2015.404.

(34) Ding, D.; Solís-Fernández, P.; Hibino, H.; Ago, H. Spatially Controlled Nucleation of Single-Crystal Graphene on Cu Assisted by Stacked Ni. *ACS Nano* **2016**, *10* (12), 11196–11204. https://doi.org/10.1021/acsnano.6b06265.

(35) Magnuson, C. W.; Kong, X.; Ji, H.; Tan, C.; Li, H.; Piner, R.; Ventrice, C. A.; Ruoff, R. S. Copper Oxide as a "Self-Cleaning" Substrate for Graphene Growth. *J. Mater. Res.* **2014**, *29* (3), 403–409. https://doi.org/DOI: 10.1557/jmr.2013.388.

(36) Pang, J.; Bachmatiuk, A.; Fu, L.; Yan, C.; Zeng, M.; Wang, J.; Trzebicka, B.; Gemming, T.; Eckert, J.; Rummeli, M. H. Oxidation as A Means to Remove Surface Contaminants on Cu Foil Prior to Graphene Growth by Chemical Vapor Deposition. *J. Phys. Chem. C* **2015**, *119* (23), 13363–13368. https://doi.org/10.1021/acs.jpcc.5b03911.

(37) Strudwick, A. J.; Weber, N. E.; Schwab, M. G.; Kettner, M.; Weitz, R. T.; Wünsch, J. R.; Müllen, K.; Sachdev, H. Chemical Vapor Deposition of High Quality Graphene Films from Carbon Dioxide Atmospheres. *ACS Nano* **2015**, *9* (1), 31–42.

https://doi.org/10.1021/nn504822m.

(38) Kraus, J.; Böbel, M.; Günther, S. Suppressing Graphene Nucleation during CVD on Polycrystalline Cu by Controlling the Carbon Content of the Support Foils. *Carbon N. Y.* **2016**, *96*, 153–165. https://doi.org/https://doi.org/10.1016/j.carbon.2015.09.048.

(39) Choubak, S.; Biron, M.; Levesque, P. L.; Martel, R.; Desjardins, P. No Graphene Etching in Purified Hydrogen. *J. Phys. Chem. Lett.* **2013**, *4* (7), 1100–1103. https://doi.org/10.1021/jz400400u.

(40) Tao, L.; Guangyu, H.; Guowei, H.; Yuhan, K.; Weifei, F.; Hongzheng, C.; Qi, W.; Hideo, I.; Daisuke, F.; Yingchun, L.; et al. Graphene Nucleation Preferentially at Oxygen-Rich Cu Sites Rather Than on Pure Cu Surface. *Adv. Mater.* **2015**, *27* (41), 6404–6410. https://doi.org/10.1002/adma.201501473.

(41) Braeuninger-Weimer, P.; Brennan, B.; Pollard, A. J.; Hofmann, S. Understanding and Controlling Cu-Catalyzed Graphene Nucleation: The Role of Impurities, Roughness, and Oxygen Scavenging. *Chem. Mater.* **2016**, *28* (24), 8905–8915. https://doi.org/10.1021/acs.chemmater.6b03241.

(42) Reckinger, N.; Tang, X.; Joucken, F.; Lajaunie, L.; Arenal, R.; Dubois, E.; Hackens, B.; Henrard, L.; Colomer, J.-F. Oxidation-Assisted Graphene Heteroepitaxy on Copper Foil. *Nanoscale* **2016**, *8* (44), 18751–18759. https://doi.org/10.1039/C6NR02936A.

(43) Zhu, L. F.; Zou, J.; Li, Z.; Li, X.; Wang, K.; Wei, J.; Zhong, M.; Wu, D.; Xu, Z.; Hongwei. Topology Evolution of Graphene in Chemical Vapor Deposition, a Combined Theoretical/Experimental Approach toward Shape Control of Graphene Domains.

Nanotechnology **2012**, *23* (11), 115605.

(44) Wofford, J. M.; Nie, S.; McCarty, K. F.; Bartelt, N. C.; Dubon, O. D. Graphene Islands on Cu Foils: The Interplay between Shape, Orientation, and Defects. *Nano Lett.* **2010**, *10* (12), 4890–4896. https://doi.org/10.1021/nl102788f.

(45) Zhiqiang, L.; Ting, Y.; Jingzhi, S.; Yingying, W.; Sanhua, L.; Lei, L.; G., G. G.; Zexiang, S.; Jianyi, L. Large-Scale Synthesis of Bi-layer Graphene in Strongly Coupled Stacking Order. *Adv. Funct. Mater.* **2011**, *21* (5), 911–917. https://doi.org/10.1002/adfm.201002227.

(46) Li, X.; Cai, W.; An, J.; Kim, S.; Nah, J.; Yang, D.; Piner, R.; Velamakanni, A.; Jung, I.; Tutuc, E.; et al. Large-Area Synthesis of High-Quality and Uniform Graphene Films on Copper Foils. *Science (80-.).* **2009**, *324*, 1312.

(47) Lancellotti, L.; Bobeico, E.; Capasso, A.; Lago, E.; Delli Veneri, P.; Leoni, E.; Buonocore, F.; Lisi, N. Combined Effect of Double Antireflection Coating and Reversible Molecular Doping on Performance of Few-Layer Graphene/n-Silicon Schottky Barrier Solar Cells. *Sol. Energy* **2016**, *127* (Supplement C), 198–205. https://doi.org/https://doi.org/10.1016/j.solener.2016.01.036.

(48) Santangelo, S.; Messina, G.; Malara, A.; Lisi, N.; Dikonimos, T.; Capasso, A.; Ortolani, L.; Morandi, V.; Faggio, G. Taguchi Optimized Synthesis of Graphene Films by Copper Catalyzed Ethanol Decomposition. *Diam. Relat. Mater.* **2014**, *41*, 73–78. https://doi.org/10.1016/j.diamond.2013.11.006.

(49) Capasso, A.; De Francesco, M.; Leoni, E.; Dikonimos, T.; Buonocore, F.; Lancellotti, L.; Bobeico, E.; Sarto, M. S.; Tamburrano, A.; De Bellis, G.; et al. Cyclododecane as Support

Material for Clean and Facile Transfer of Large-Area Few-Layer Graphene. *Appl. Phys. Lett.* **2014**, *105* (11), 113101. https://doi.org/10.1063/1.4895733.

(50) Meca, E.; Lowengrub, J.; Kim, H.; Mattevi, C.; Shenoy, V. B. Epitaxial Graphene Growth and Shape Dynamics on Copper: Phase-Field Modeling and Experiments. *Nano Lett.* **2013**, *13* (11), 5692–5697. https://doi.org/10.1021/nl4033928.

(51) Jinkins, K.; Camacho, J.; Farina, L.; Wu, Y. Examination of Humidity Effects on Measured Thickness and Interfacial Phenomena of Exfoliated Graphene on Silicon Dioxide via Amplitude Modulation Atomic Force Microscopy. *Appl. Phys. Lett.* **2015**, *107* (24), 243107. https://doi.org/10.1063/1.4938068.

(52) Nemes-Incze, P.; Osváth, Z.; Kamarás, K.; Biró, L. P. Anomalies in Thickness Measurements of Graphene and Few Layer Graphite Crystals by Tapping Mode Atomic Force Microscopy. *Carbon N. Y.* **2008**, *46* (11), 1435–1442. https://doi.org/http://dx.doi.org/10.1016/j.carbon.2008.06.022.

(53) Jung, W.; Park, J.; Yoon, T.; Kim, T.-S.; Kim, S.; Han, C.-S. Prevention of Water Permeation by Strong Adhesion Between Graphene and SiO2 Substrate. *Small* **2014**, *10* (9), 1704–1711. https://doi.org/10.1002/smll.201302729.

(54) Ferrari, A. C.; Meyer, J. C.; Scardaci, V.; Casiraghi, C.; Lazzeri, M.; Mauri, F.; Piscanec, S.; Jiang, D.; Novoselov, K. S.; Roth, S.; et al. Raman Spectrum of Graphene and Graphene Layers. *Phys. Rev. Lett.* **2006**, *97* (18), 187401. https://doi.org/10.1103/PhysRevLett.97.187401.

(55) Malard, L. M.; Pimenta, M. A.; Dresselhaus, G.; Dresselhaus, M. S. Raman Spectroscopy

in Graphene. *Phys. Rep.* **2009**, *473* (5), 51–87. https://doi.org/http://dx.doi.org/10.1016/j.physrep.2009.02.003.

(56) Goniszewski, S.; Adabi, M.; Shaforost, O.; Hanham, S. M.; Hao, L.; Klein, N. Correlation of P-Doping in CVD Graphene with Substrate Surface Charges. *Sci. Rep.* **2016**, *6*, 22858.

(57) Xu, H.; Chen, Y.; Zhang, J.; Zhang, H. Investigating the Mechanism of Hysteresis Effect in Graphene Electrical Field Device Fabricated on SiO2 Substrates Using Raman Spectroscopy. *Small* **2012**, *8* (18), 2833–2840. https://doi.org/10.1002/smll.201102468.

(58) Xiang, S.; Miseikis, V.; Planat, L.; Guiducci, S.; Roddaro, S.; Coletti, C.; Beltram, F.; Heun, S. Low-Temperature Quantum Transport in CVD-Grown Single Crystal Graphene. *Nano Res.* **2016**, *9* (6), 1823–1830. https://doi.org/10.1007/s12274-016-1075-0.

(59) Wang, G.; Zhang, M.; Zhu, Y.; Ding, G.; Jiang, D.; Guo, Q.; Liu, S.; Xie, X.; Chu, P. K.; Di, Z.; et al. Direct Growth of Graphene Film on Germanium Substrate. *Sci. Rep.* **2013**, *3*, 2465.

(60) Petrone, N.; Dean, C. R.; Meric, I.; van der Zande, A. M.; Huang, P. Y.; Wang, L.; Muller, D.; Shepard, K. L.; Hone, J. Chemical Vapor Deposition-Derived Graphene with Electrical Performance of Exfoliated Graphene. *Nano Lett.* **2012**, *12* (6), 2751–2756. https://doi.org/10.1021/nl204481s.

(61) Zhang, Y.; Zhang, L.; Kim, P.; Ge, M.; Li, Z.; Zhou, C. Vapor Trapping Growth of Single-Crystalline Graphene Flowers: Synthesis, Morphology, and Electronic Properties. *Nano Lett.* **2012**, *12* (6), 2810–2816. https://doi.org/10.1021/nl300039a.

(62) Chin, H.-T.; Lee, J.-J.; Hofmann, M.; Hsieh, Y.-P. Impact of Growth Rate on Graphene

Lattice-Defect Formation within a Single Crystalline Domain. *Sci. Rep.* **2018**, *8* (1), 4046. https://doi.org/10.1038/s41598-018-22512-5.

(63) Zhao, P.; Kumamoto, A.; Kim, S.; Chen, X.; Hou, B.; Chiashi, S.; Einarsson, E.; Ikuhara, Y.; Maruyama, S. Self-Limiting Chemical Vapor Deposition Growth of Monolayer Graphene from Ethanol. *J. Phys. Chem. C* **2013**, *117* (20), 10755–10763. https://doi.org/10.1021/jp400996s.